Supplemental Figures

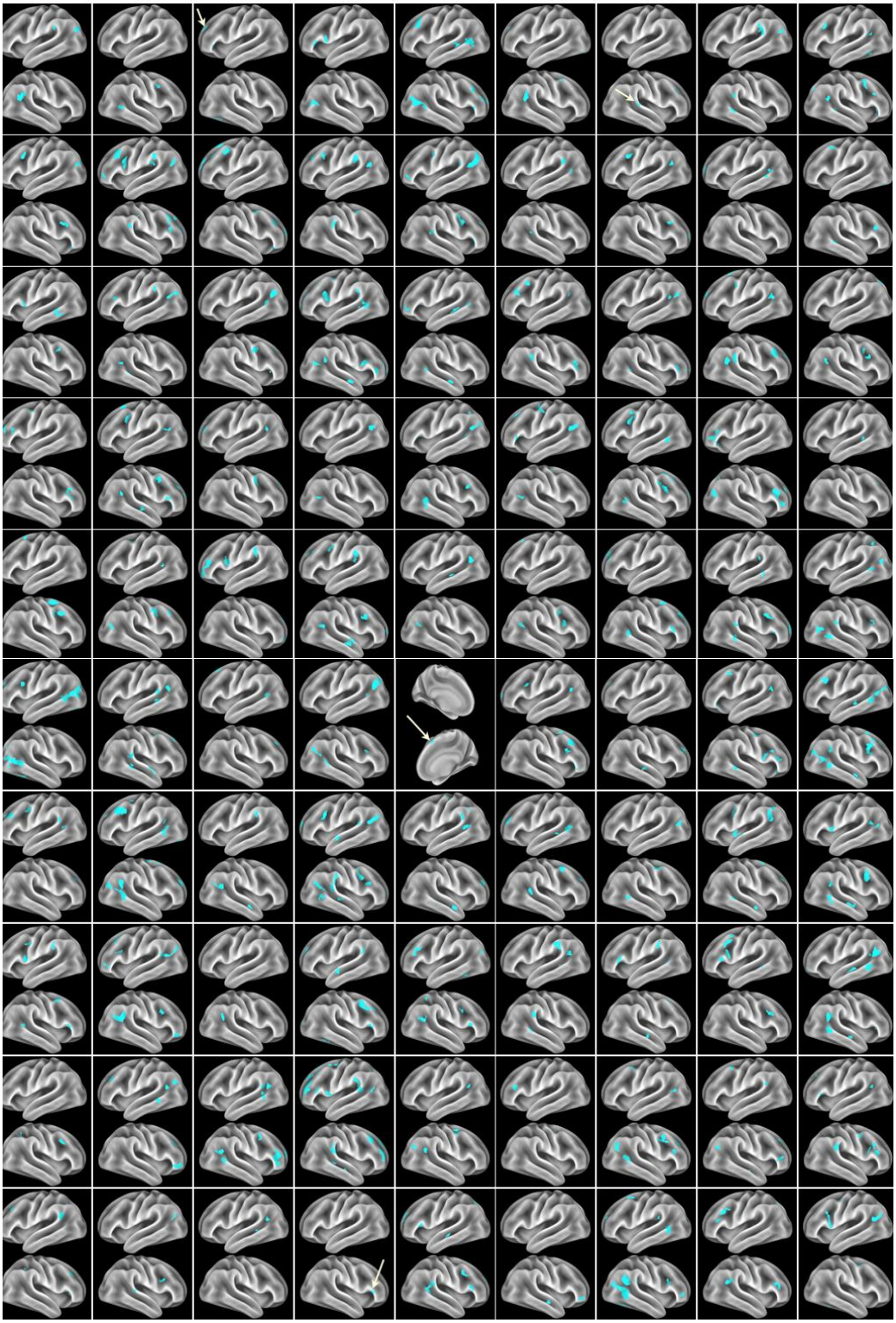

SI Figure 1: Network variants are present in all individuals. Network variants are present in each individual included in the study. The figure displays binarized variants (light blue) for all MSC individuals and 81 randomly selected HCP subjects. Variants were created by use of a

conservative fixed threshold of spatial correlations less than 0.15 (rather than lowest decile as used in the main text, to determine if low similarity locations were present in all individuals). Size and SNR exclusion criteria were also applied, as described in the methods.

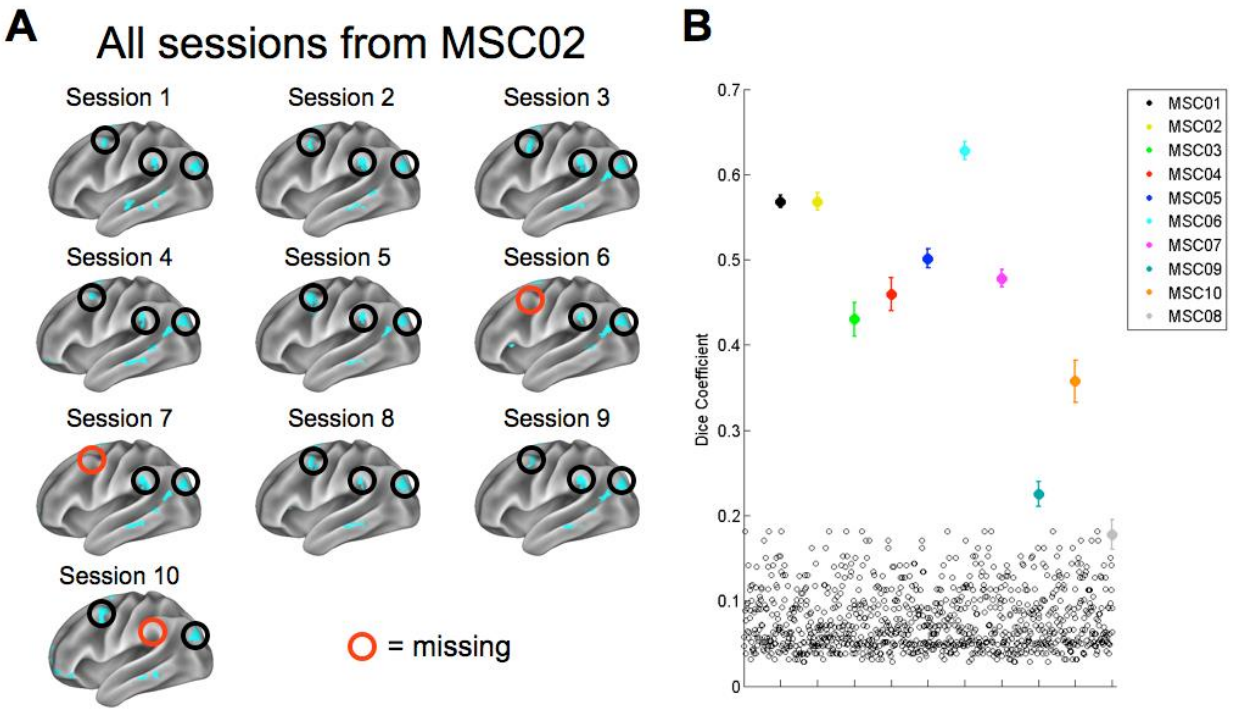

SI Figure 2: Reliability of binarized network variants. The figure shows the session-to-session reliability of binarized network variants within each MSC individual. (A) Binary variants for all 10 sessions from MSC02 are displayed. Most variants are consistent across sessions, with a few missing variants highlighted (red circle; note that these often still showed relatively low spatial correlations, as in Fig. 2, but did not pass the threshold to be in the lowest decile for that session). (B) We quantified the reliability of variant locations across sessions within an individual using the dice coefficient instead of the intraclass correlation (ICC), since the data are binary. The mean and standard error of within-subject variant reliability (i.e., mean +/- SE across all 10 sessions) is shown for each individual. The open black circles represent the null distribution of variant reliability. To create the null, we performed 1000 random permutations of pairs of sessions drawn from two different MSC individuals (with replacement). Only MSC08 shows a dice coefficient in the range of between subject variant dice.

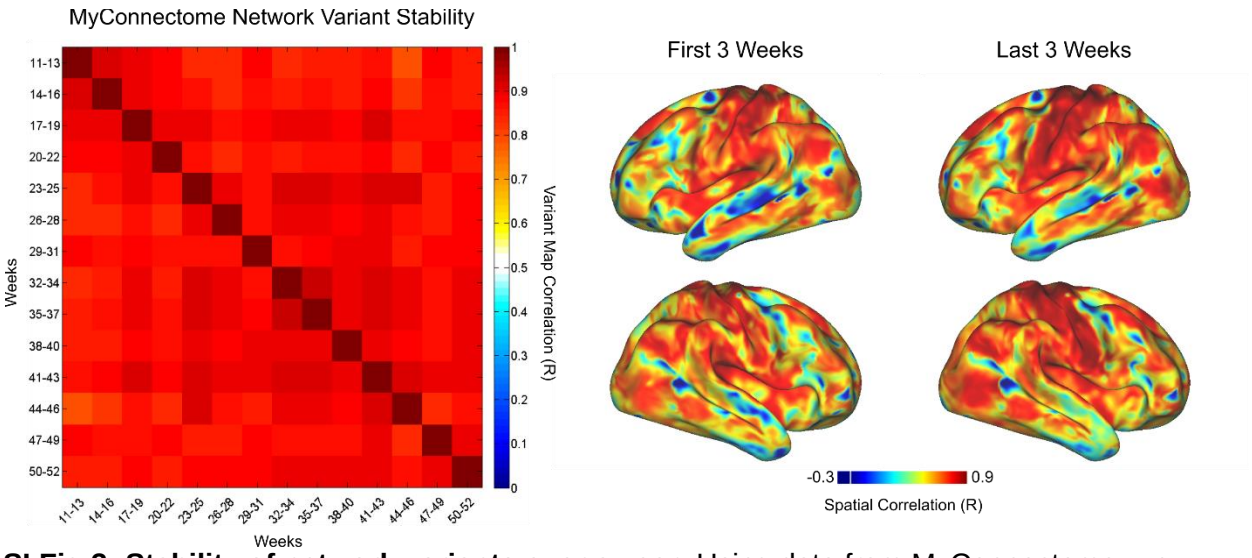

SI Fig 3: Stability of network variants over a year. Using data from MyConnectome, we tested the stability of network variants over a year in a single individual. The correlation matrix on the left demonstrates that the individual's network variants (i.e., the spatial correlation maps) are quite stable from month-to-month (data from all sessions within a 3 week block are concatenated together). The brains on the right show that the individual's network variants are extremely similar (r = 0.85) at the beginning and end of the year.

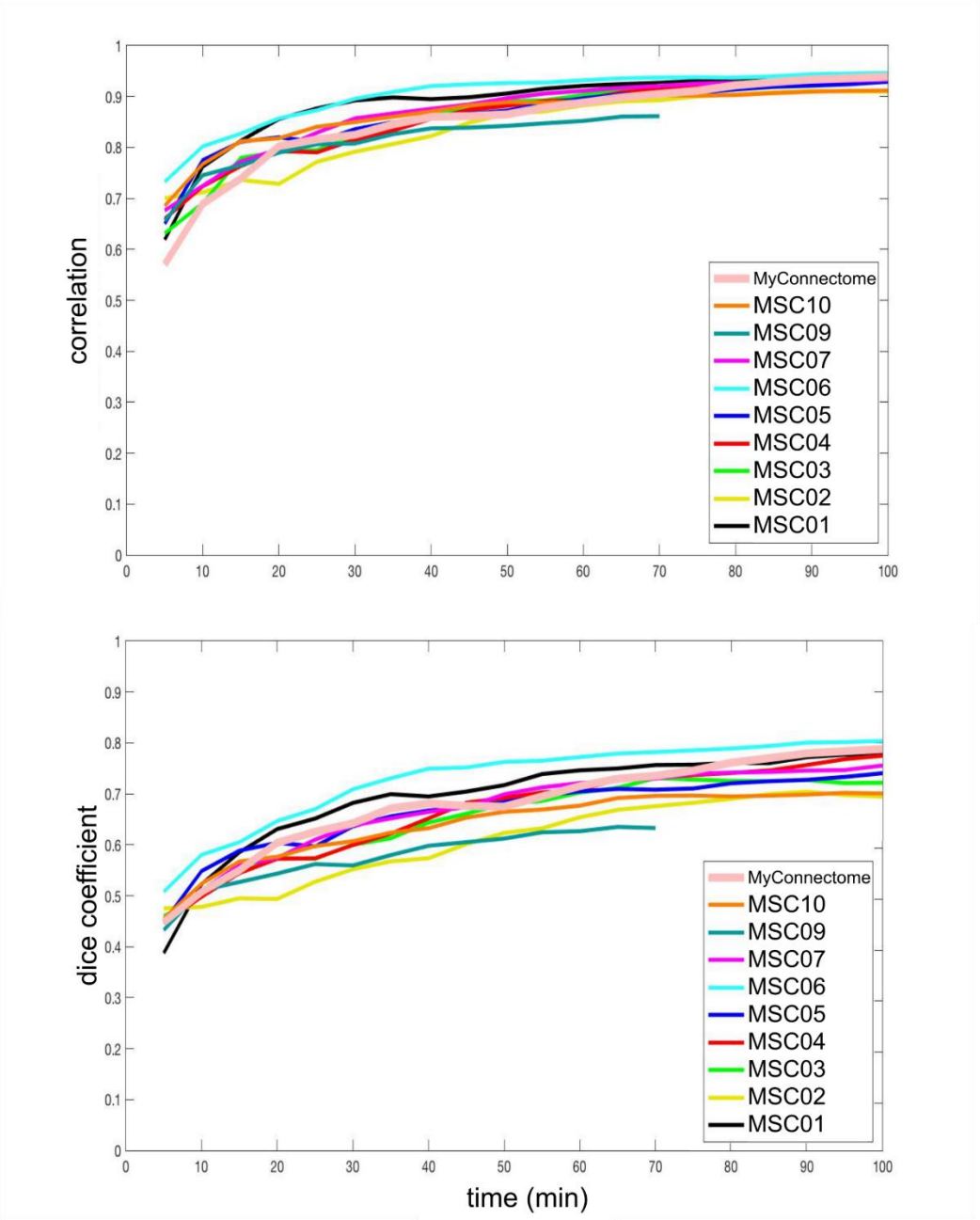

SI Figure 4: Sampling variability affects identification of network variants. To quantify the effects of sampling variability on network variants, data from both the MSC and MyConnectome individuals were used. Split-halves of the data were generated, and the BOLD time series in one of the split-halves was sampled consecutively in 5-minute increments. Network variants were identified via a spatial correlation between the individual and the group-average data (as in Figure 1). Then, at each 5-minute increment, both the spatial correlation map (top) and the map of binarized network variants (bottom; lowest decile of spatial correlation map, SNR and size exclusion applied) were compared to the corresponding map generated from the remaining "true" half of the data (as in (Evan M. Gordon et al., 2017; Laumann et al., 2015)). Spatial correlation maps were compared via Pearson correlation and binarized maps were compared via dice overlap. To prevent an artificial inflation of the dice coefficient due to the large number

of vertices that did not contain variants, only vertices that were classified as variants in at least one of the split-halves were considered.

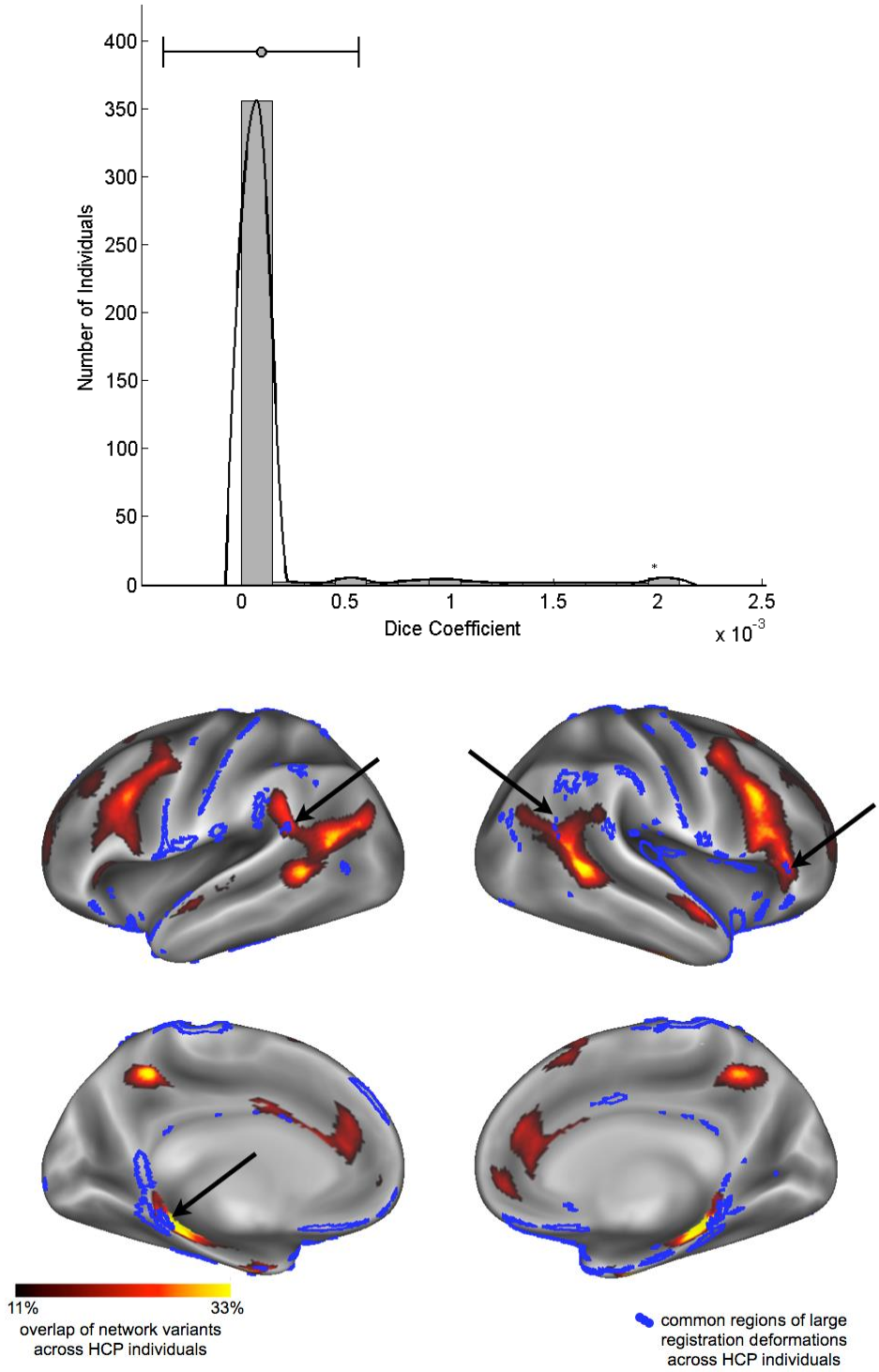

SI Figure 5: Overlap of network variants and surface registration deformations. The distribution (top) displays the dice coefficient overlap between an individual's network variants and large deformations (both contractions and expansions) that occurred during surface registration, a proxy measure of anatomical variability, across the HCP dataset. Large

deformations are defined as the top decile of the absolute value of the areal distortion map, an output from the HCP registration procedure (registering the individual's FreeSurfer defined-surface to the Conte69 atlas; (Glasser et al., 2013)). There is little to no overlap between network variants and registration deformations within individuals. Common regions of registration deformations across HCP individuals (>30% of individuals) are displayed as blue borders on the brains (bottom), with the scale bar showing the overlap of network variants across HCP subjects (reproduced from Figure 3A). There is minimal overlap between common locations for network variants and common locations for large deformations across individuals (black arrows).

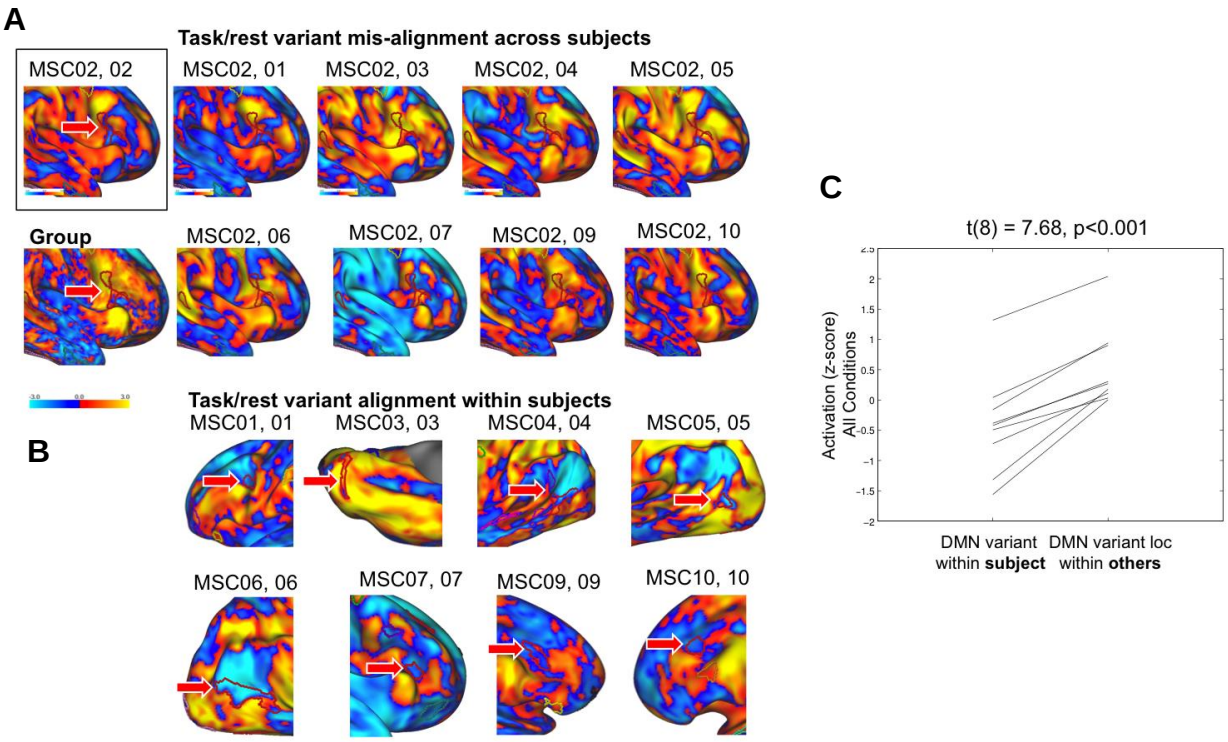

SI Figure 6: Task-rest alignment of DMN variants. (A) Alignment of a DMN variant from MSC02 to task activations from all other subjects. Note that while MSC02 shows deactivations in this variant, other participants and the group show primarily activations. (B) DMN variants in other participants also align with deactivations during mixed design tasks. (C) DMN variants from a given subject show significantly lower activations than the same location from other subjects (each line represents a single subject).

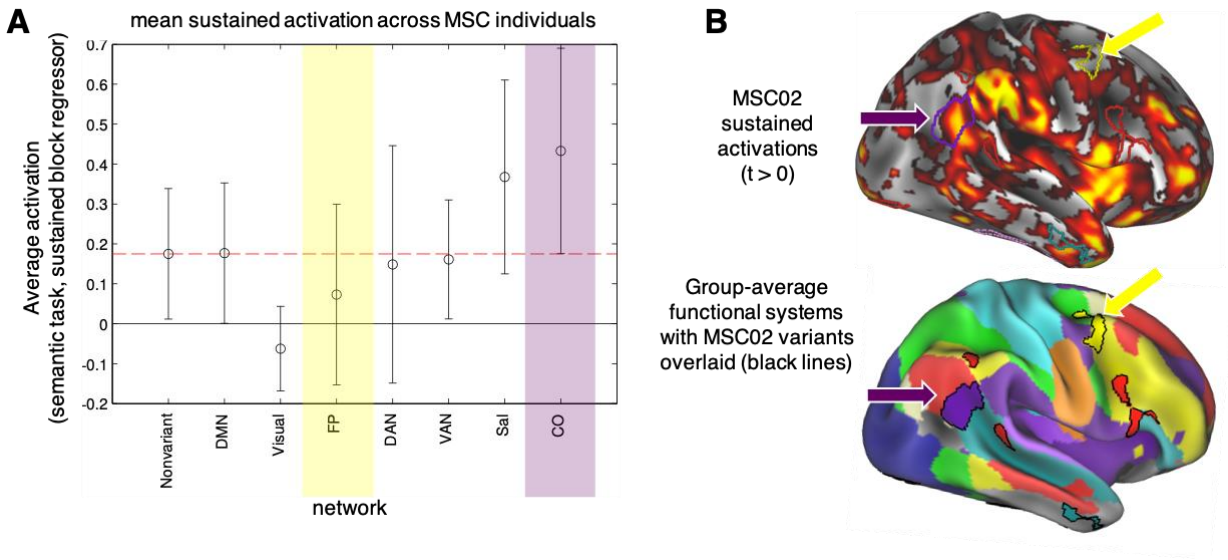

SI Figure 7: Sustained activation in cinguloopercular variants. Task-evoked activations during a mixed design task are displayed for network variants. The mean and standard error across the 9 included highly sampled subjects reveals that sustained activations (all conditions – baseline) are stronger in cinguloopercular variants specifically. Example sustained activations ($t > 0$) are displayed for subject MSC02 with outlines of the subject's variants overlaid (as in Figure 4). Note that there is strong activation in the cinguloopercular variant near the angular gyrus (purple arrow), whereas there is no activation in the frontoparietal variant near the superior frontal gyrus (yellow arrow). The group-average functional networks with the same variants overlaid are displayed below for reference (variants shown with black outlines).

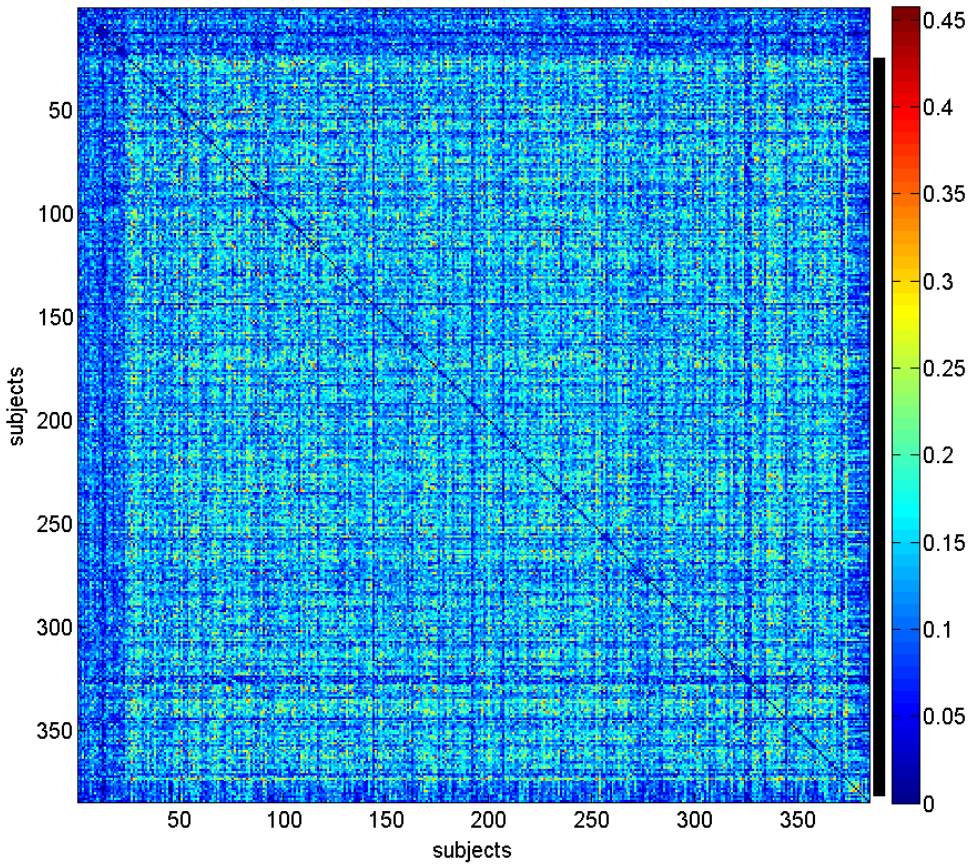

SI Figure 8: Clustering via anatomical location of network variants. The matrix displays the dice coefficient overlap between the locations of network variants in all pairs of individuals (i.e., the degree to which two individuals both have variants 1, 2, and 3 and both do not have variants 4, 5, and 6). The matrix is sorted by clusters, with unlabeled subjects in the first portion of the matrix. Across InfoMap thresholds (see Methods), individuals cluster into one large group (solid black line). Thus, we did not find evidence for sub-groups of individuals with similar anatomical distributions of network variants.

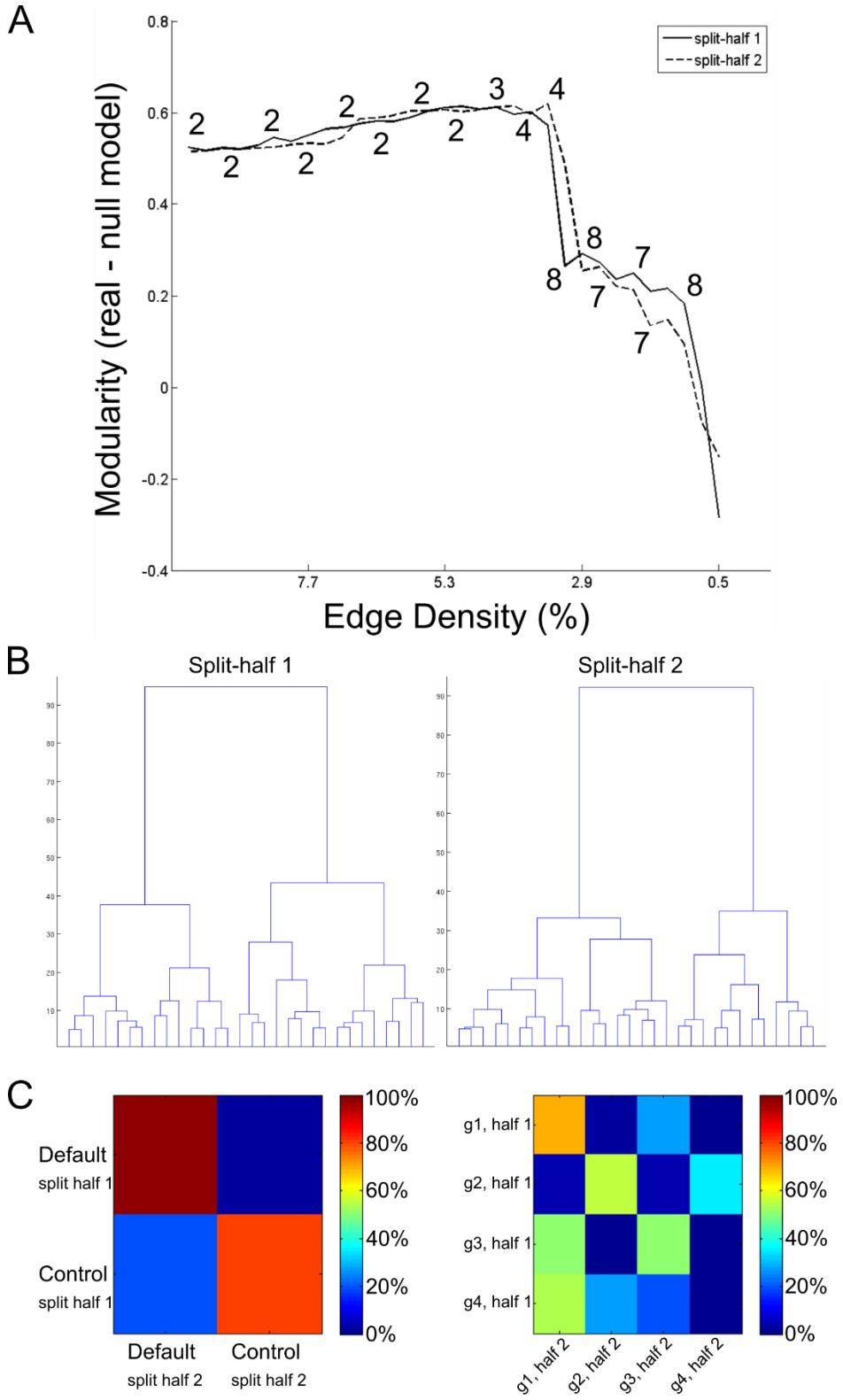

SI Figure 9: Validation of the sub-group clustering. We validated the clustering of individuals in two sub-groups (**Fig 5** in the main text) via two methods: (1) modularity versus a null model that preserves the degree distribution and (2) hierarchical clustering. **(A)** The number of clusters found by InfoMap (see Methods in the main text) varies as a function of edge density. Thus, for

each edge density we tested the modularity of the real solution against a null model. The null model is a random network (at that specific edge density) with the same degree distribution as the real network (generated via the Brain Connectivity Toolbox function null_model_und_sign.m; (Rubinov and Sporns, 2010)). The two sub-group solution was the most robust across edge density thresholds and split-halves, as indicated by the numbers near the lines. **(B)** The dendrograms produced by hierarchical clustering (created via MATLAB functions dendrogram and linkage, Ward's minimum variance method) are displayed for each split-half. The cophentic correlation coefficient was greater than 0.8 for each split-half. **(C)** A confusion matrix was generated for the two- and four-group hierarchical clustering solutions to test their reliability across each split-half. If split-half 1 is the 'true answer,' then the confusion matrix represents the degree to which split-half 2 matches the true answer (in terms of sub-group labeling). In order to align sub-group labels across each split-half (e.g., to ensure that individuals in the default sub-group are labeled with a 1 in each split-half), the average network template match was used (i.e., the line graphs in Figure 5 in the main text). The two sub-group solution had a much higher percentage of true positives and a much lower percentage of false positives and false negatives than the four sub-group solution.

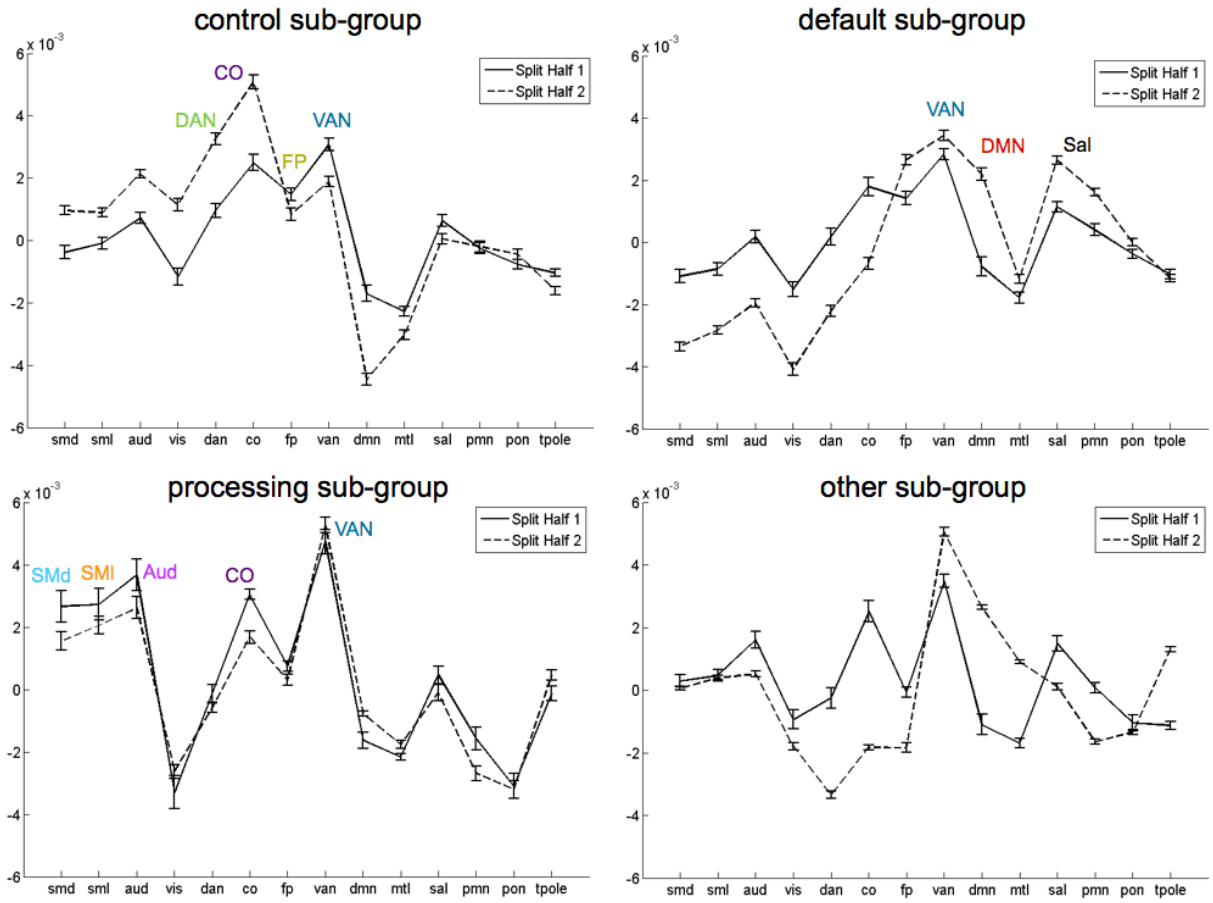

SI Figure 10: The four sub-group solution. The four sub-groups of individuals from the HCP dataset, identified via patterns of network variants, are displayed. Individuals in these sub-groups have variants that are more like the frontoparietal, dorsal attention, and cinguloopercular networks (top left), the default mode, frontoparietal, and ventral attention networks (top right),

the motor, auditory, ventral attention, and cinguloopercular networks (bottom left), or a mixed pattern (bottom right).

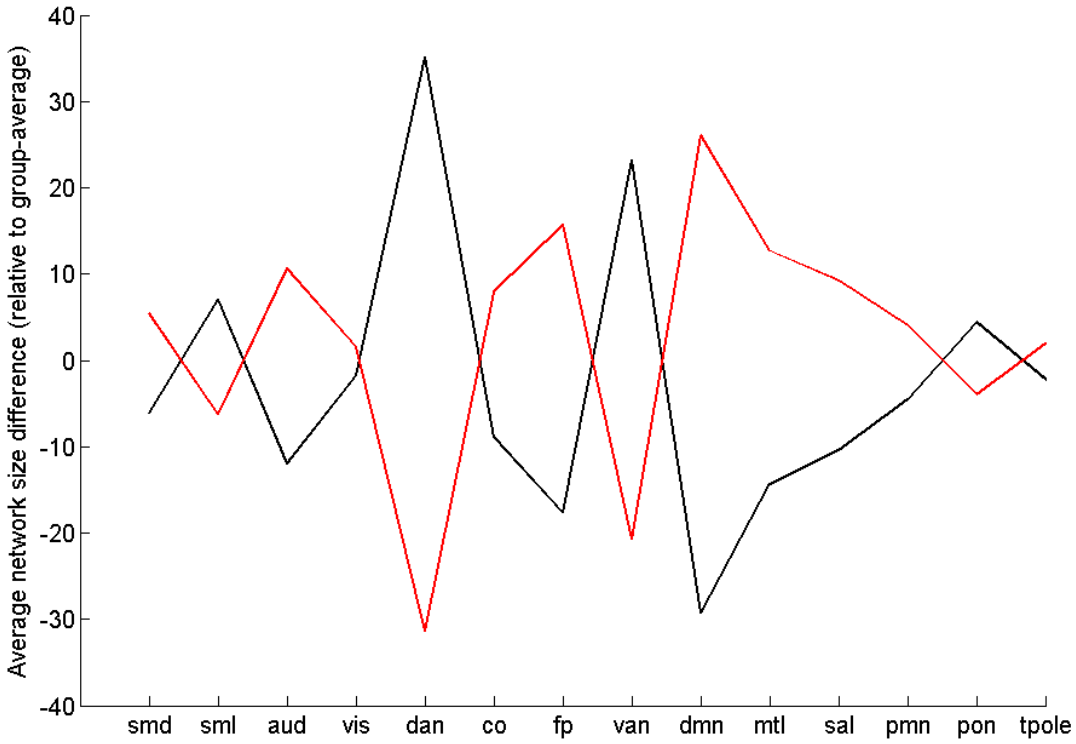

SI Figure 11: Group-wise differences in the size of each network. The solid line represents the mean expansion or contraction of each functional network in individuals in the two sub-groups identified in the main results (black = control and processing, red = default). The specific measure is the number of surface vertices assigned to each network in the individual minus the same number for the group-average. A positive number means more vertices assigned to that network than the group-average (an expansion), a negative number means fewer vertices assigned to that network than the group-average (a contraction), and zero means an identical number of vertices assigned to that network as the group-average. The pattern is partially consistent with that observed in **Fig 5B**, but sub-group differences are driven by the dorsal and ventral attention networks versus the default mode, salience, and frontoparietal networks.

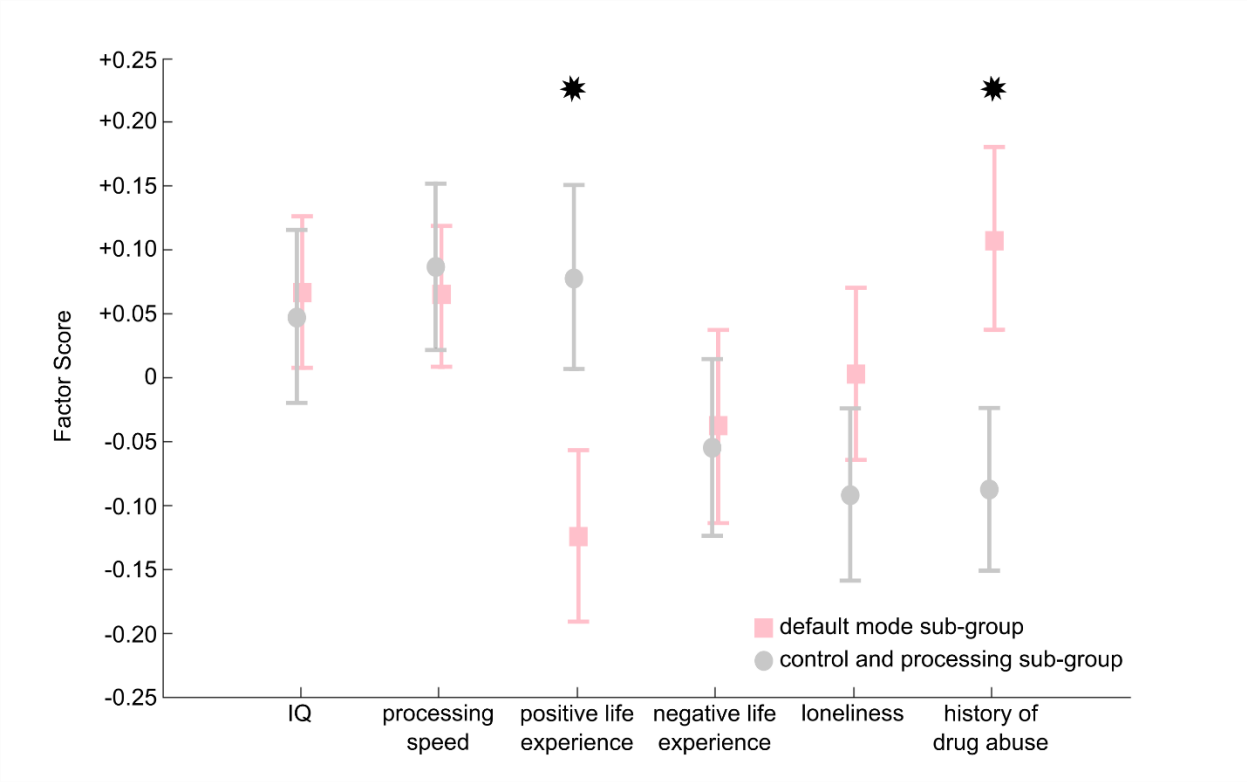

SI Figure 12: Group-wise differences in neuropsychological measures. Factor scores derived from the HCP behavioral measures are displayed (mean and standard error) for the two larger sub-groups from the HCP dataset (**Fig 5B**). Factor scores for the control and processing sub-group were significantly higher in the Positive Life Experience factor ($t(344) = 2.038$) and significantly lower in the History of Drug Abuse factor ($t(344) = -2.039$) than scores for the default sub-group. Two-sample *t*-tests were performed with subjects from both split-halves grouped together.

Supplemental Methods

Acquisition details

Three datasets are included in this manuscript: the first contains five hours of resting-state data from each of 10 highly-sampled individual subjects, referred to as the Midnight Scan Club or MSC dataset; the second includes 14 hours of resting-state data from a single individual collected over the course of a year, referred to as the MyConnectome dataset; and, the third includes one hour of resting-state data from 384 unrelated individuals from the Human Connectome Project 1200 subject release, referred to as the HCP dataset.

Briefly, for the MSC and WashU 120, high-resolution T1-weighted, T2-weighted, and resting-state BOLD data were collected on a Siemens 3T Magnetom Tim Trio with a 12-channel head coil (gradient-echo EPI sequence, isotropic 4 mm^3 voxels, TE of 27ms, and TR of 2.2s and 2.5s, respectively; (Evan M Gordon et al., 2017; Power et al., 2013)). The MyConnectome dataset was acquired on a Siemens 3T Skyra with a 32-channel head coil (multi-band sequence with MB factor 4, isotropic 2.4 mm^3 voxels, TE of 30ms, and TR of 1.16s; (Laumann et al., 2015; Poldrack et al., 2015)). The HCP was collected on a custom Siemens 3T Skyra with a custom 32-channel head coil (multi-band sequence with MB factor 8, isotropic 2 mm^3 voxels, TE of 33ms, and TR of 0.72s (Van Essen et al., 2012)).

We excluded all subjects whose resting-state BOLD runs contained large to moderate amounts of head motion in order to ensure reliable identification of network variants. Thus, we excluded data from one MSC individual with a substantial amount of head motion and drowsiness (Evan M. Gordon et al., 2017; Laumann et al., 2016). We included all high-quality (low-motion) MyConnectome sessions after the schedule shift to Tuesday and Thursday acquisitions, following Laumann and colleagues (Laumann et al., 2015). A total of 84 sessions were included. Exclusion criteria for individuals from the full HCP 1200-subject HCP release were as follows: (1) we removed duplicates and subjects who did not complete the study; (2) we required subjects to have >75% of their data, i.e. 45 minutes, retained post motion censoring (see description of censoring procedures below); (3) we required that all subjects be unrelated (if more than one family member passed the previous criteria, the subject with the most data was selected). Thus, 384 HCP subjects were included. From these 384 individuals, two split-halves were created for within-dataset replication of our findings. Split-halves were balanced on the factors of age, sex, handedness, race, mean frames retained post motion censoring, and years of education. See **SI Table 1** for full details.

HCP subject exclusion criteria

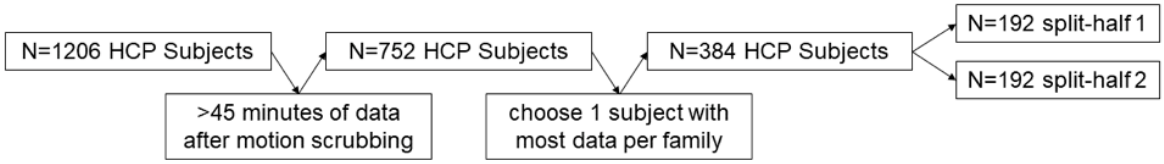

Split-half demographics

Group	N (N male)	N Right Handed	N Caucasian	N African American	N Asian	N Mixed or Unknown	N Hispanic	Mean (+/- std) Age in Years	Mean (+/- std) Frames Retained post-scrubbing	Mean (+/- std) Years of Education
Split Half 1	192 (87M)	120	129	24	13	4	22	28.4 +/- 3.7	4324 +/- 322	15.0 +/- 1.7
Split Half 2	192 (87M)	120	129	25	12	5	21	28.4 +/- 3.6	4332 +/- 324	15.0 +/- 1.8
t-test (382 degrees of freedom)	p = 1 t = 0	p = 1 t = 0	p = 0.951 t = 0.062					p = 0.945 t = 0.070	p = 0.815 t = -0.234	p = 0.815 t = 0.235

SI Table 1: HCP exclusion criteria and split-halves. The flow diagram at the top shows the exclusion criteria applied to obtain the final set of 384 HCP subjects. The table shows demographic variables on which the split-halves were balanced, as well as t-tests for each variable.

Functional preprocessing

For each subject, the volumetric BOLD time series from each run were concatenated together. Slice timing correction was applied first (but not in the HCP dataset, per recommendation from Glasser et al., 2013). Then, all functional data were aligned to the first frame of the first run using rigid body transforms, after which they were normalized to a whole-brain mode of 1000 (Miezin et al., 2000). For the WashU 120 and HCP, the functional data were registered to the high-resolution T1 image. Following this, a one-step operation (Smith et al., 2004) was applied to resample (3 cubic mm) and register the data to the 711-2B atlas (Ojemann et al., 1997). For the MSC, the functional data were first registered to the T2 image and then to the T1 image, which was separately registered to the template space. Finally, field inhomogeneity distortion correction was applied using the mean field map applied to all sessions (Evan M. Gordon et al., 2017; Laumann et al., 2015). Distortion correction was not applied to the WashU 120 because field maps were not collected.

In order to remove further artifacts additional preprocessing was applied (Power et al., 2014). Frame-wise displacement (FD) was calculated (Power et al., 2012), and frames with FD greater than 0.2 mm were flagged for censoring for the MSC and WashU 120 datasets. However, the increased temporal resolution of the HCP acquisition (0.72s TR) caused respiration artifacts to alias into the FD trace (Siegel et al., 2017). Thus, the 6 realignment (motion) parameters were filtered with a lowpass filter at 0.1 Hz before calculating FD values. The filtered FD threshold for frame censoring was 0.1 mm. Uncensored segments with fewer than 5 contiguous frames were

also flagged for censoring as well. First, the aligned and registered BOLD data were demeaned and detrended. Multi-linear nuisance regression was implemented with 36 regressors: the whole-brain mean, individually defined white matter and ventricular CSF signals, the temporal derivatives of each of these regressors, and an additional 24 movement regressors derived by expansion (Friston et al., 1996; Satterthwaite et al., 2013). Then, the previously flagged frames were removed and interpolated over using least squares spectral estimation (Power et al., 2014). Finally, the data were bandpass filtered from 0.009-0.08 Hz. The MyConnectome data were processed identically to the MSC data, except the FD threshold was 0.25 mm.

Volume-to-surface mapping and functional connectivity processing

Unsmoothed (but otherwise completely processed) BOLD data were mapped to each individual's native midthickness surface via the ribbon-constrained sampling procedure (Connectome Workbench v1.0) (Marcus et al., 2013). Then, the mapped data were registered to the fsaverage surface in one step using the deformation map generated from the aforementioned shape-based spherical registration. Afterwards, a geodesic Gaussian smoothing kernel was applied (FWHM = 6 mm, sigma = 2.55) to the surface registered data (Gordon et al., 2016). Subcortical and cerebellar data were not considered in any further analyses due to substantial signal-to-noise issues in HCP data.

Before computing correlations (functional connectivity), the first 30 seconds of each functional run (14, 41, and 12 frames, for the MSC, HCP, and WashU-120, respectively) were discarded to account for magnetization equilibrium and an auditory evoked response to the start of the EPI sequence in addition to frame censoring (Laumann et al., 2015). For the MyConnectome data, the first 60 seconds of each run (52 frames) were discarded due to an amplified evoked response as a function of noise cancelling headphones.

Task data processing

In this study, we focus on activations in the two mixed design (Petersen and Dubis, 2012) tasks from the MSC dataset: the semantic task and the coherence task. Briefly, the semantic task required a noun or verb judgment on a series of presented words, while the coherence task required a yes/no judgment regarding whether an array of dots was arranged concentrically on the screen (Glass, 1969). Blocks of each task consisted of start cues signaling the beginning of the block, followed by a series of randomly intermixed trials in each condition (nouns and verbs in the semantic task, 0% and 50% coherence arrays in the coherence task).

Task activations were modeled with in-house imaging analysis software (IDL) using a general linear model (GLM) approach as previously described (Evan M. Gordon et al., 2017; Gratton et al., 2018). Eight time-points were modeled for cues and each trial type in each condition. In addition, block regressors for sustained activations were included across the full task block. MSC individuals completed two runs of each task in each of their 10 sessions; each individual was analyzed separately.

Behavioral measures

Demographic variables included education recoded into fewer categories to avoid small cell sizes (≤high school graduate, some college, ≥4-year college graduate), employment (not

working, part time, full time), family income, also recoded into fewer categories (bottom quartile ≤$29,999, median $30,000-49,999, 3rd quartile $50,000-74,999, 4th quartile >$75,000), and whether the respondent was still in school or taking courses for a degree (Yes/No), was married or in a live-in relationship (Yes/No), and was born in Missouri (Yes/No). Race/ethnicity was recoded per NIH guidelines – not Hispanic White (n=814, 67.5%), Black/African American (n=191, 15.84%), Asian (n=68, 5.64%), American Indian/mixed/unknown (n=28, 2.32%; there were only n=2 American Indian individuals), and Hispanic/Latino (n=105, 8.71%) – and dummy coded (not Hispanic White vs all others, Black/African American vs all others, etc).

Cognitive variables included all measures from the NIH Toolbox Cognition Battery (Picture Vocabulary, Oral Reading Recognition, the Flanker Task, Dimensional Change Card Sort, List Sorting, Picture Sequence Memory, and Pattern Completion Processing Speed; (Weintraub et al., 2013)) in addition to the number of correct responses from the Penn Progressive Matrices (Bilker et al., 2012), the Variable Short Penn Line Orientation, the Penn Word Memory Test, true positives from the Short Penn Continuous Performance Test (Gur et al., 2010), and Delay Discounting Area Under the Curve for $200 and $40,000 (Estle et al., 2006; Myerson et al., 2001). Cognitive variables were Z-score normalized across all HCP subjects and were not adjusted for age or sex to allow flexibility in covariate adjustment in other analyses.

Emotion variables included all NIH Toolbox surveys (Anger-Affect, Anger-Hostility, Anger-Physical Aggression, Fear-Affect, Fear-Somatic Arousal, Sadness, General Life Satisfaction, Meaning and Purpose, Positive Affect, Friendship, Loneliness, Perceived Hostility, Perceived Rejection, Emotional Support, Instrumental Support, Perceived Stress, and Self-Efficacy). They were Z-score normalized and also not adjusted for age or sex. Drug use variables were derived from SSAGA interviews on lifetime use and captured lifetime quantity/severity of use: history of alcohol abuse or dependence (Yes/No); number of cigarettes smoked: never smoked (0 cigarettes), experimented (1-19 cigarettes), occasional use (20-99 cigarettes), regular use (≥100 cigarettes); number of times used cannabis (never, 1, ≥2); and number of times used each of cocaine, hallucinogens, opiates, sedatives, or stimulants (never, ≥1).

For each behavior category, relationships between variables were examined using Pearson or polychoric/tetrachoric correlations for continuous and categorical variables, respectively. If a variable did not have a correlation of ≥0.32 with at least one other variable, which would suggest ~10% shared variance, that variable was excluded from consideration. Oblique rotation was always tested first and was retained if inter-factor correlations were significantly different from zero at $p<0.05$ (uncorrected). Final EFA structure was determined based on a combination of indicators including: (1) factor eigenvalues and scree plot; (2) variables had high loadings (≥0.32, accounting for approximately 10% of factor variance) on at least one factor; (3) variables had high loadings on one factor and relatively low loadings on all other factors, i.e., cross-loading was minimal; (4) at least two variables had high loadings on a factor; and (5) interpretability (Tabachnick and Fidell, 2007). Factor scores were output for use in subsequent analyses. Internal consistency of the factors was assessed using estimates of the squared multiple correlations (SMCs) of variables with each factor, where factor scores are predicted from the observed variables. SMCs vary from 0 to 1 and high SMCs (≥0.7) indicate that observed variables account for significant factor score variance. All data manipulation and EFA analysis was conducted in SAS 9.2 (SAS Institute Inc., 2008, Cary, NC, USA).

EFA results

Demographic variables (final n=1199): Whether a respondent was born in Missouri did not correlate with other variables and was not further considered. Being Black/African American was related to three other demographic variables and this dummy variable was retained for analysis. EFA resulted in a single factor. Being in school or employed had low factor loadings and these variables were dropped from analysis. The four remaining variables (income, education, relationship status, and Black/African American) had inadequate internal consistency (SMC=0.59) suggesting that as a group, these variables are poor indicators of an underlying construct. We suggest that these variables be considered separately.

Cognitive variables (final n=1193): The two delay discounting variables correlated only with each other (r=0.675) and not with any other variables. In addition, the partial correlation remained high (r=0.65) after controlling for all other variables suggesting that delay discounting does not share variance with the other cognitive measures and was therefore not considered further. Likewise, Penn continuous performance and word memory tests did not correlate with any other variables and were not considered further. The picture sequence task had low loadings on all factors and was excluded. The final EFA consisted of two factors (**SI Table 2**). Variables that loaded highly on the first factor reflected fluid intelligence, reading and comprehension, spatial orientation and working memory; we named this factor General IQ. Processing speed variables loaded highly on the second factor which we named Processing Speed. The inter-factor correlation was 0.40 suggesting that higher general IQ is related to higher processing speed. The General IQ and Processing Speed factors had good to fair internal consistency (SMCs=0.80 and 0.65, respectively).

Cognition (n=1193)	**General IQ**	**Processing Speed**	
Card sort based on color or shape	0.06	**0.66**	
Flanker inhibitory control	0.00	**0.64**	
Progressive matrices	**0.63**	0.03	
Oral reading recognition	**0.79**	-0.03	
Picture vocabulary	**0.78**	-0.06	
Processing speed - pattern comparison	0.01	**0.54**	
Variable short line orientation	**0.50**	0.13	
List sorting working memory	**0.45**	0.08	
Internal consistency	0.80	0.65	
Inter-factor correlation	*0.40*		
Emotion (n=1204)	**Negative**	**Positive**	**Loneliness**
Anger - affect	**0.73**	-0.02	0.09
Fear - affect	**0.82**	-0.08	-0.08
Fear - somatic arousal	**0.59**	0.14	0.01
Sadness	**0.65**	**-0.32**	-0.02
Life satisfaction	-0.02	**0.71**	-0.02
Meaning and purpose	0.04	**0.69**	-0.05
Positive affect	-0.09	**0.64**	-0.03
Friendship	0.09	0.29	**-0.53**
Loneliness	0.18	-0.28	**0.46**
Perceived hostility	**0.34**	0.21	**0.56**
Perceived rejection	0.22	0.04	**0.70**
Emotional social support	0.16	**0.34**	**-0.60**
Instrumental social support	0.15	**0.33**	**-0.38**
Perceived stress	**0.49**	**-0.33**	0.10
Self-efficacy	-0.12	**0.43**	-0.08
Internal consistency	0.87	0.83	0.82
Inter-factor correlations			
Positive	*-0.53*		
Loneliness	*0.49*	*-0.57*	
Lifetime Drug Use (n=1204)	**Quantity/Frequency**		
Alcohol abuse or dependence	**0.50**		
Number of cigarettes (0, 1-19, 20-99, ≥100)	**0.50**		
Cocaine (0, ≥1)	**0.65**		
Hallucinogens (0, ≥1)	**0.67**		
Opiates (0, ≥1)	**0.66**		
Sedatives (0, ≥1)	**0.60**		
Stimulants (0, ≥1)	**0.66**		
Marijuana (0, 1, ≥2)	**0.60**		
Internal consistency	0.82		

SI Table 2. Exploratory factor analysis of HCP behavioral variables. Factor loadings for the cognition, emotion, and substance use variables are displayed. Loadings of at least 0.32 (accounting for approximately 10% of factor variance) are bolded. Internal consistency of the factors is shown at the bottom of each factor loading vector, and inter-factor correlations are shown where applicable.

Emotion variables (final n=1204): The variables anger-hostility and anger-physical aggression had low factor loadings and were excluded. The final EFA solution consisted of three factors (**SI Table 2**). Fear, anger, sadness, perceived social hostility and stress loaded on the first factor which we call Negative. Life satisfaction, meaning and purpose, social support, and self-efficacy loaded on the second factor which we call Positive. The third factor was characterized by positive loadings of loneliness and perceived social hostility and rejection, and negative loadings of social support and social relationship and we call this factor Loneliness. Higher score on the Negative factor was related to higher score on the Loneliness factor and higher score on the

Positive factor was related to lower scores on both Negative and Loneliness factors. All three factors had good internal consistency (SMCs=0.87, 0.83, and 0.82, respectively).

Drug use variables (final n=1204): Drug use variables comprised a single factor that captured overall quantity and heaviness of use. This factor had good internal consistency (SMC=0.82).

Statistical analysis of behavior

Analysis of the variance of behavioral factor scores explained by network variant group assignment was conducted in MATLAB R2012a using the Statistics and Machine Learning Toolbox multi-linear regression (MathWorks Inc., 2012, Natick, MA, USA). Factor scores were modeled as dependent variables and variant group as the independent variable of interest. Regressions were performed both including and excluding other covariates, which included age, sex, handedness, and number of frames retained post-scrubbing. Further, *t*-tests were used to compare differences in factor scores between sub-groups, with an FDR correction for multiple comparisons.

Supplemental References

Bilker, W.B., Hansen, J.A., Brensinger, C.M., Richard, J., Gur, R.E., Gur, R.C., 2012. Development of Abbreviated Nine-Item Forms of the Raven's Standard Progressive Matrices Test. Assessment 19, 354–369. doi:10.1177/1073191112446655

Estle, S.J., Green, L., Myerson, J., Holt, D.D., 2006. Differential effects of amount on temporal and probability discounting of gains and losses. Mem. Cogn. 34, 914–928. doi:10.3758/BF03193437

Friston, K.J., Williams, S., Howard, R., Frackowiak, R.S.J., Turner, R., 1996. Movement-related effects in fMRI time-series. Magn. Reson. Med. 35, 346–355. doi:10.1002/mrm.1910350312

Glass, L., 1969. Moiré effect from random dots. Nature 223, 578–580. doi:10.1038/223578a0

Glasser, M.F., Sotiropoulos, S.N., Wilson, J.A., Coalson, T.S., Fischl, B., Andersson, J.L., Xu, J., Jbabdi, S., Webster, M., Polimeni, J.R., Van Essen, D.C., Jenkinson, M., 2013. The minimal preprocessing pipelines for the Human Connectome Project. Neuroimage 80, 105–124. doi:10.1016/j.neuroimage.2013.04.127

Gordon, E.M., Laumann, T.O., Adeyemo, B., Huckins, J.F., Kelley, W.M., Petersen, S.E., 2016. Generation and Evaluation of a Cortical Area Parcellation from Resting-State Correlations. Cereb. Cortex 26, 288–303. doi:10.1093/cercor/bhu239

Gordon, E.M., Laumann, T.O., Gilmore, A.W., Newbold, D.J., Greene, D.J., Berg, J.J., Ortega, M., Hoyt-Drazen, C., Gratton, C., Sun, H., Hampton, J.M., Coalson, R.S., Nguyen, A.L., McDermott, K.B., Shimony, J.S., Snyder, A.Z., Schlaggar, B.L., Petersen, S.E., Nelson, S.M., Dosenbach, N.U.F., 2017. Precision Functional Mapping of Individual Human Brains. Neuron 95, 791–807.e7. doi:10.1016/j.neuron.2017.07.011

Gordon, E.M., Laumann, T.O., Gilmore, A.W., Petersen, S.E., Nelson, S.M., Dosenbach, N.U.F., Gordon, E.M., Laumann, T.O., Gilmore, A.W., Newbold, D.J., Greene, D.J., 2017. Precision Functional Mapping of Individual Human NeuroResource Precision Functional Mapping of Individual Human Brains. Neuron 95, 1–17. doi:10.1016/j.neuron.2017.07.011

Gratton, C., Laumann, T.O., Nielsen, A.N., Greene, D.J., Gordon, E.M., Gilmore, A.W., Nelson, S.M., Coalson, R.S., Snyder, A.Z., Schlaggar, B.L., Dosenbach, N.U.F., Petersen, S.E., 2018. Functional Brain Networks Are Dominated by Stable Group and Individual Factors, Not Cognitive or Daily Variation. Neuron. doi:10.1016/j.neuron.2018.03.035

Gur, R.C., Richard, J., Hughett, P., Calkins, M.E., Macy, L., Bilker, W.B., Brensinger, C., Gur, R.E., 2010. A cognitive neuroscience-based computerized battery for efficient measurement of individual differences: Standardization and initial construct validation. J. Neurosci. Methods 187, 254–262. doi:10.1016/j.jneumeth.2009.11.017

Laumann, T.O., Gordon, E.M., Adeyemo, B., Snyder, A.Z., Joo, S.J., Chen, M.-Y., Gilmore, A.W., McDermott, K.B., Nelson, S.M., Dosenbach, N.U.F., Schlaggar, B.L., Mumford, J.A., Poldrack, R.A., Petersen, S.E., 2015. Functional System and Areal Organization of a Highly Sampled Individual Human Brain. Neuron 1–14. doi:10.1016/j.neuron.2015.06.037

Laumann, T.O., Snyder, A.Z., Mitra, A., Gordon, E.M., Gratton, C., Adeyemo, B., Gilmore, A.W., Nelson, S.M., Berg, J.J., Greene, D.J., McCarthy, J.E., Tagliazucchi, E., Laufs, H., Schlaggar, B.L., Dosenbach, N.U.F., Petersen, S.E., 2016. On the Stability of BOLD fMRI Correlations. Cereb. Cortex 1–14. doi:10.1093/cercor/bhw265

Marcus, D.S., Harms, M.P., Snyder, A.Z., Jenkinson, M., Wilson, J.A., Glasser, M.F., Barch, D.M., Archie, K.A., Burgess, G.C., Ramaratnam, M., Hodge, M., Horton, W., Herrick, R., Olsen, T., McKay, M., House, M., Hileman, M., Reid, E., Harwell, J., Coalson, T., Schindler, J., Elam, J.S., Curtiss, S.W., Van Essen, D.C., 2013. Human Connectome Project informatics: Quality control, database services, and data visualization. Neuroimage 80, 202–219. doi:10.1016/j.neuroimage.2013.05.077

Miezin, F.M., Maccotta, L., Ollinger, J.M., Petersen, S.E., Buckner, R.L., 2000. Characterizing the hemodynamic response: Effects of presentation rate, sampling procedure, and the possibility of ordering brain activity based on relative timing. Neuroimage 11, 735–759. doi:10.1006/nimg.2000.0568

Myerson, J., Green, L., Warusawitharana, M., 2001. Area under the curve as a measure of discounting. J. Exp. Anal. Behav. 76, 235–243. doi:10.1901/jeab.2001.76-235

Ojemann, J.G., Akbudak, E., Snyder, A.Z., McKinstry, R.C., Raichle, M.E., Conturo, T.E., 1997. Anatomic localization and quantitative analysis of gradient refocused echo-planar fMRI susceptibility artifacts. Neuroimage 6, 156–167. doi:10.1006/nimg.1997.0289

Petersen, S.E., Dubis, J.W., 2012. The mixed block/event-related design. Neuroimage. doi:10.1016/j.neuroimage.2011.09.084

Poldrack, R.A., Laumann, T.O., Koyejo, O., Gregory, B., Hover, A., Chen, M.Y., Gorgolewski, K.J., Luci, J., Joo, S.J., Boyd, R.L., Hunicke-Smith, S., Simpson, Z.B., Caven, T., Sochat, V., Shine, J.M., Gordon, E., Snyder, A.Z., Adeyemo, B., Petersen, S.E., Glahn, D.C., Mckay, D.R., Curran, J.E., Göring, H.H.H., Carless, M.A., Blangero, J., Dougherty, R., Leemans, A., Handwerker, D.A., Frick, L., Marcotte, E.M., Mumford, J.A., 2015. Long-term neural and physiological phenotyping of a single human. Nat. Commun. 6. doi:10.1038/ncomms9885

Power, J., Schlaggar, B., Lessov-Schlaggar, C., Petersen, S., 2013. Evidence for hubs in human functional brain networks. Neuron 79, 798–813. doi:10.1016/j.neuron.2013.07.035

Power, J.D., Barnes, K.A., Snyder, A.Z., Schlaggar, B.L., Petersen, S.E., 2012. Spurious but systematic correlations in functional connectivity MRI networks arise from subject motion. Neuroimage 59, 2142–2154. doi:10.1016/j.neuroimage.2011.10.018

Power, J.D., Mitra, A., Laumann, T.O., Snyder, A.Z., Schlaggar, B.L., Petersen, S.E., 2014. Methods to detect, characterize, and remove motion artifact in resting state fMRI. Neuroimage 84, 320–341. doi:10.1016/j.neuroimage.2013.08.048

Rubinov, M., Sporns, O., 2010. Complex network measures of brain connectivity: Uses and interpretations. Neuroimage 52, 1059–1069. doi:10.1016/j.neuroimage.2009.10.003

Satterthwaite, T.D., Elliott, M.A., Gerraty, R.T., Ruparel, K., Loughead, J., Calkins, M.E., Eickhoff, S.B., Hakonarson, H., Gur, R.C., Gur, R.E., Wolf, D.H., 2013. An improved framework for confound regression and filtering for control of motion artifact in the preprocessing of resting-state functional connectivity data. Neuroimage 64, 240–256. doi:10.1016/j.neuroimage.2012.08.052

Siegel, J.S., Mitra, A., Laumann, T.O., Seitzman, B.A., Raichle, M., Corbetta, M., Snyder, A.Z., 2017. Data quality influences observed links between functional connectivity and behavior. Cereb. Cortex 27, 4492–4502. doi:10.1093/cercor/bhw253

Smith, S.M., Jenkinson, M., Woolrich, M.W., Beckmann, C.F., Behrens, T.E.J., Johansen-Berg, H., Bannister, P.R., De Luca, M., Drobnjak, I., Flitney, D.E., Niazy, R.K., Saunders, J., Vickers, J., Zhang, Y., De Stefano, N., Brady, J.M., Matthews, P.M., 2004. Advances in functional and structural MR image analysis and implementation as FSL, in: NeuroImage. doi:10.1016/j.neuroimage.2004.07.051

Tabachnick, B.G., Fidell, L.S., 2007. Using Multivariate Statistics, 5th ed. Allyn and Bacon, Boston, MA.

Van Essen, D.C., Ugurbil, K., Auerbach, E., Barch, D., Behrens, T.E.J., Bucholz, R., Chang, A., Chen, L., Corbetta, M., Curtiss, S.W., Della Penna, S., Feinberg, D., Glasser, M.F., Harel, N., Heath, A.C., Larson-Prior, L., Marcus, D., Michalareas, G., Moeller, S., Oostenveld, R., Petersen, S.E., Prior, F., Schlaggar, B.L., Smith, S.M., Snyder, A.Z., Xu, J., Yacoub, E., 2012. The Human Connectome Project: A data acquisition perspective. Neuroimage 62, 2222–2231. doi:10.1016/j.neuroimage.2012.02.018

Weintraub, S., Dikmen, S.S., Heaton, R.K., Tulsky, D.S., Zelazo, P.D., Bauer, P.J., Carlozzi, N.E., Slotkin, J., Blitz, D., Wallner-Allen, K., Fox, N.A., Beaumont, J.L., Mungas, D., Nowinski, C.J., Richler, J., Deocampo, J.A., Anderson, J.E., Manly, J.J., Borosh, B., Havlik, R., Conway, K., Edwards, E., Freund, L., King, J.W., Moy, C., Witt, E., Gershon, R.C., 2013. Cognition assessment using the NIH Toolbox. Neurology 80, S54–S64. doi:10.1212/WNL.0b013e3182872ded